Charge-state dependence of inner-shell processes in collisions between highly charged Xe ions and solids at intermediate energies

Jieru Ren,[1,2] Yongtao Zhao,[1,3,*] Xianming Zhou,[1,2] Xing Wang,[1,3] Yu Lei,[1] Ge Xu,[1,2] Rui Cheng,[1] Yuyu Wang,[1] Shidong Liu,[1,2] Yuanbo Sun,[1,2] and Guoqing Xiao[1]

[1]*Plasma Physics Department, Institute of Modern Physics, CAS, Lanzhou, 730000, China*

[2]*School of Physics, University of Chinese Academy of Sciences, Beijing, 100049, China*

[3]*School of Science, Xi'an Jiaotong University, Xi'an, 710049, China*

(Received 27 August 2015; published 11 December 2015)

The x-ray emission during the penetration of 2–6 MeV Xe^{q+} ($q = 20,22,26,30$) ions into thick solid targets of iron and nickel has been measured. An obvious charge-state and incident-energy dependence of the target-to-projectile vacancy-production cross-section ratios was found for the iron target but not for the nickel target. The results are supported by the vacancy-sharing model and direct ionization theory and imply the great importance of level matching for the inner-shell process. The charge equilibration time of Xe^{30+} in solid iron was derived to be around 9 fs from the measured x-ray yields.

DOI: 10.1103/PhysRevA.92.062710 PACS number(s): 34.35.+a, 34.50.Fa, 34.70.+e

I. INTRODUCTION

Inner-shell processes in highly charged ion-atom collisions are very complicated due to the many-body nature of the system. This is especially true for slow collisions characterized by impact velocities smaller than the typical orbital velocities of inner-shell electrons. In slow collisions, short-lived quasimolecules are formed; hence the electron promotion via quasimolecular level crossings [1,2] must be taken into account in addition to the direct Coulomb ionization and excitation [3,4]. A great deal of investigation has been done on the vacancy production process in heavy-ion-atom collisions involving collisions in the energy region of typically 0.5 MeV/u or more in recent decades [5–12]. In the extremely low energy region of about tens of eV/u, considerable progress has also been made through techniques such as Auger spectroscopy, x-ray spectroscopy, etc. [13–15]. However, relatively little attention has been directed towards the collisions at an energy of tens of keV/u with projectiles as heavy as xenon.

Early work involving 326–470 MeV xenon ions and 40 keV to 1.1 MeV copper ions with various targets were reported by Meyerhof *et al.* and Anholt *et al.*, respectively, in a series of papers [16–19]. A noted feature is that the projectile vacancy production cross section shows a very pronounced cyclic dependence on the target atomic number. A similar phenomenon was observed in heavy-ion-atom collisions for 5 MeV Xe ions [20]. The projectile vacancy production cross section is greatly enhanced when the binding energies of the projectile and the target match up. This led to a long-lasting intense investigation of the inner-shell vacancy production mechanism near the level-matching region [21–25].

Since the binding energy of the highly charged ion sensitively depends on the charge state, changing the charge state is another way to finely adjust the binding energy to achieve level matching except for choosing suitable projectile and target combinations. In the present work, we systematically changed the charge state of incident xenon ions to control the binding energy near the K-L level-matching region to obtain insight into the atomic process taking place in the investigated energy region.

As the projectiles penetrate into the target, they will soon reach the equilibrium charge state. Knowledge of the charge equilibration time of highly charged ions inside solids is very important for the study of atomic collision. Hattass *et al.* [26] found that when the slow highly charged ions Xe^{44+} ($0.5 \times 10^6 < v < 10^6$ m/s) penetrate into a solid target, they will deposit their potential energy into the nanometer-scale target volumes on the time scale of 7 fs and then reach the equilibrium charge state. Herrmann *et al.* [27] showed that the preequilibrium length was only one atomic layer, through the investigation of the charge-state dependence of the energy loss of 576 keV argon ions inside the carbon foil. Fang *et al.* [28] proved that the charge equilibration time of 0.8 MeV/u uranium ions in carbon foil was less than 5.4 fs through the measurement of the projectile charge-state distribution after the ions passed through the carbon foil. In the present work, we try to probe the charge equilibration time through the investigation of x-ray emission during the collision of highly charged xenon ions with a solid target at intermediate energies.

In this context, the x-ray emission spectra are presented as a function of the projectile charge state and incident energy. The experimental results are discussed in terms of the vacancy sharing in the framework of the quasimolecular model and direct ionization theory. Finally, the charge equilibration time of highly charged ions in a solid is estimated.

II. EXPERIMENTAL SETUP

The experiment was performed at the 320 kV electron cyclotron resonance (ECR) ion source platform at the Institute of Modern Physics (IMP) in Lanzhou. Highly charged ions were directed by two quadrupole lenses towards the target chamber after momentum analysis in a 90° bending magnet. The pressure in the chamber was kept below 10^{-8} mbar. Highly charged ions impacted on the solid target at normal incidence. The target thickness is of millimeter magnitude, much larger than the range of the projectile, which is only about hundreds of nanometers. The measured x rays are from both the preequilibrium and equilibrium stages.

*zhaoyt@impcas.ac.cn; zhaoyongtao@mail.xjtu.edu.cn

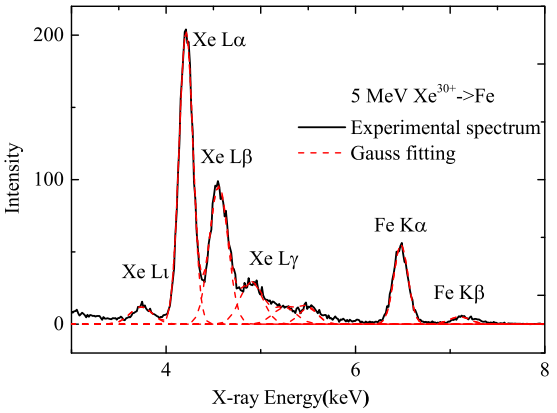

FIG. 1. (Color online) A typical x-ray spectrum for 5 MeV Xe^{30+} ions impacting on an iron target.

Emitted x rays were detected by a silicon drift detector at 135° with respect to the ion beam axis subtending a solid angle of 1.1 msr. The number of incident ions on the target was monitored over time with a calibrated transmitting Faraday cup. The details have been presented in Ref. [29]. The efficiency of the detector was provided by the manufacturer, and for x-ray energies ranging from 4 to 8 keV, the detection efficiency is larger than 97%. The energy calibration was done with a ^{55}Fe source. A typical spectrum, which was measured in the experiment, is shown in Fig. 1. It can been seen that the Xe L and Fe K lines are quite well resolved.

III. RESULTS AND DISCUSSION

A. Charge-state effect

Figure 2 shows the normalized experimental spectra for an Fe target induced by Xe^{20+}, Xe^{22+}, Xe^{26+}, and Xe^{30+} ions with incident energy of 5 MeV. The spectra are normalized to 10^{11} incident ions. An obvious charge-state effect was observed. Along with the increase of the charge state, a decreasing x-ray

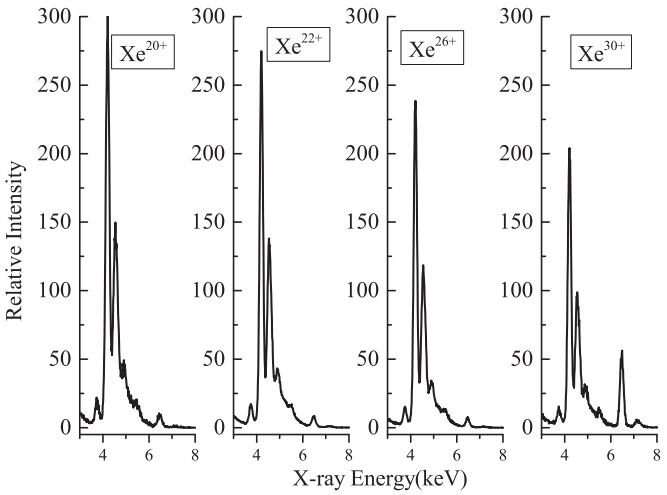

FIG. 2. Normalized x-ray spectra induced by 5 MeV $Xe^{20+,22+,26+,30+}$ impacting on an iron target.

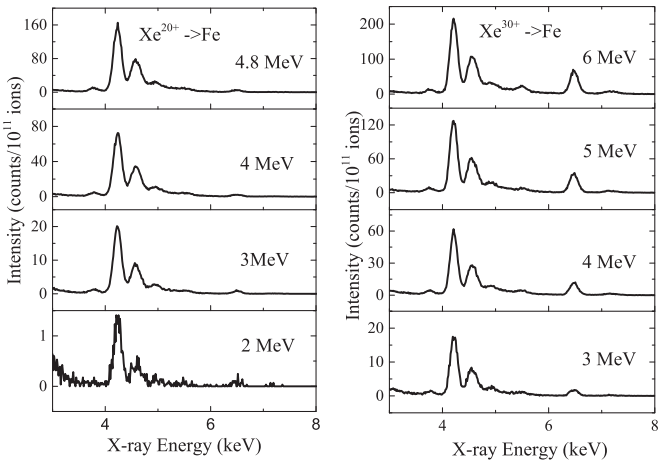

FIG. 3. Spectra for $Xe^{20+,30+}$ impacting on an iron target with various incident energies.

emission yield for Xe L lines was measured, while for Fe K lines, they showed a sharp enhancement for Xe^{30+} impact. The spectra induced by Xe^{20+} and Xe^{30+} with various incident energies are shown in Fig. 3. The target-to-projectile x-ray emission intensity increases obviously with the incident energy for Xe^{30+} impact.

For a quantitative analysis, Xe L- and Fe K-vacancy-production cross sections are deduced from the x-ray yield using the thick target formula [30]. The target-to-projectile cross-section ratios are shown in Fig. 4 along with the theoretical results by Coulomb ionization. In the theoretical calculation, the target K-vacancy-production cross sections are determined by the well-known Binary Encounter Approximation (BEA) $1s$ function developed by Gryzinski [31] using the target K-shell binding energy and projectile nuclear charge. Following the proposals by Foster *et al.* [32] and Hansen [33], the projectile L-vacancy cross sections are estimated using the united atom binding energy and effective nuclear charge into the BEA $2p$ function. This is due to the fact that Xe L vacancies actually arise from Coulomb ionization of the $3d\sigma$ molecular orbit (MO) [34]. This explains well the experimental phenomenon that the Xe L x-ray yield decreases with the incident energy, which is owing to the increasing binding energy.

The quantitative analysis shows the following: (1) The cross-section ratio for Xe^{30+} is much larger than that for Xe^{20+}. For an energy of 5 MeV, the ratio for Xe^{30+} is about 10 times larger. (2) Compared to the case for Xe^{20+}, where only a slight increase of the cross-section ratio within the error is observed, the ratio for Xe^{30+} increases sharply with rising incident energy. It is found that the cross-section ratio for Xe^{20+} agrees with the Coulomb theory in magnitude, while the ratio for Xe^{30+} is far above the theoretical expectation. This implies that for Xe^{30+}, another mechanism apart from Coulomb ionization should also play a significant role in the vacancy-production process. Many investigations show that in low-energy collisions near the level-matching region, the vacancy-sharing model usually provides a reasonable description of the vacancy-production process [35–37].

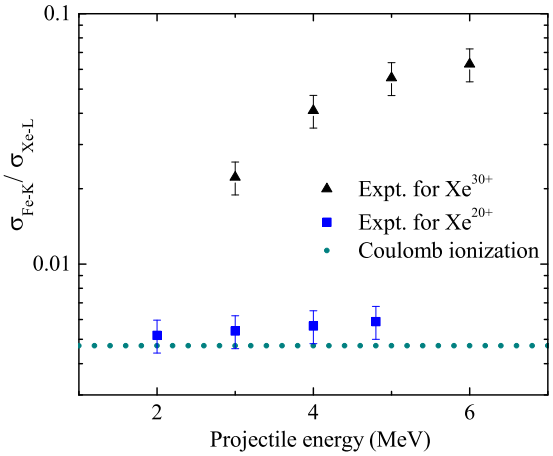

FIG. 4. (Color online) Target-to-projectile vacancy-production cross-section ratio as a function of projectile energy. The squares and triangles indicate the experimental ratio for Xe^{20+} and Xe^{30+} bombardment, respectively, and the dotted line indicates the theoretical results by Coulomb ionization.

In the framework of the vacancy-sharing model, with the help of the correlation diagram shown by Meyerhof *et al.* in Ref. [37], the Xe L_1 electron is promoted along the $3d\sigma$ MO, and on the outgoing part of the collision, the vacancies can be shared by the nearby levels such as Xe L_2, L_3 and the Fe K shell. Here we discuss only the total vacancy-production cross section of the Xe L shell. Then, taking both vacancy sharing and Coulomb ionization mechanisms into consideration, the Fe K-vacancy cross section σ_{Fe} and the Xe L-vacancy cross section σ_{Xe} can be written as

$$\sigma_{\mathrm{Fe}} = P\sigma_{3d\sigma} + \sigma_{DI}, \tag{1}$$

$$\sigma_{\mathrm{Xe}} = (1 - P)\sigma_{3d\sigma}, \tag{2}$$

where P is the vacancy-sharing probability from the $3d\sigma$ MO to the iron K level, $\sigma_{3d\sigma}$ is the $3d\sigma$ vacancy production cross section, and σ_{DI} is the iron K-vacancy-production cross section by the Coulomb ionization process.

The sharing probability P can be calculated by the Nikitin model [38]:

$$P = \frac{\exp[2\lambda(1 + \cos\theta)] - 1}{\exp(4\lambda) - 1}, \tag{3}$$

$$2\lambda = \frac{\pi|\sqrt{I_L} - \sqrt{I_K}|}{\left(\frac{1}{2}m_e v_p^2\right)^{1/2}}, \tag{4}$$

where I_L and I_K are the binding energies of the Xe L_1 shell and the Fe K shell, respectively, v_p is the projectile velocity, m_e is the electron mass, and θ is a parameter which is relevant to the dependence of the actual MO energy separation on the internuclear distance in principle. Meyerhof *et al.* [37] got a good overall fit throughout the various targets for iodine projectiles with a set of θ values on the basis of the assumption that θ is independent of the bombarding energy and target atomic number. Since in the periodic table, xenon is just next to iodine, we can take the θ value for an iodine projectile in the sharing probability calculation.

According to Eqs. (3) and (4), the parameters of the energy gap between the projectile and target shells as well as the incident energy are involved in the sharing probability calculation. Due to the high charge states of the incident ions we used, the energy levels of xenon ions depend on the charge state q, and so does the sharing probability. We plot the sharing probability as a function of the projectile charge state with a given incident energy of 5 MeV in Fig. 5(a) and plot it as a function of incident energy with given charge states of Xe^{20+} and Xe^{30+}, respectively, in Fig. 5(b).

From Fig. 5(a), where the ground-state binding energy of xenon ion is used, we see that when the binding energies of the Fe K shell (horizontal dashed line) and the Xe L_1 shell (solid curve) are totally matched, the sharing probability (stars) achieves its maximum. The investigation area in the present paper is below the matching point. Therefore, with a higher charge state, the two levels come closer to each other, which results in an increasing sharing probability P. It can be seen that the sharing probability is highly sensitive to the projectile charge state. Once the charge state increases from 20 to 30, the sharing probability P increases sharply from 0.007 to 0.144. This exactly explains the result that the cross-section ratio for Xe^{30+} is much larger than that for Xe^{20+}, which is shown in

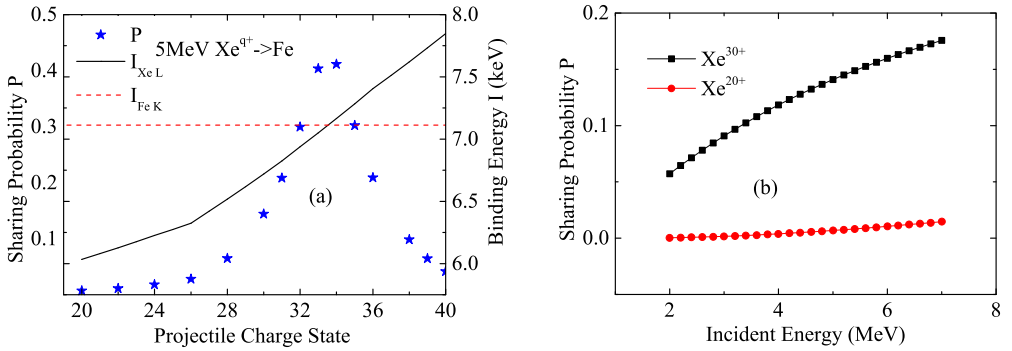

FIG. 5. (Color online) (a) Vacancy-sharing probability (left-hand scale, which is indicated by stars) for 5 MeV xenon ions striking an iron target as a function of the projectile charge state. The horizontal dashed line and the solid curve represent the binding energies of the Fe K shell and Xe L_1 shell (right-hand scale), respectively. (b) Vacancy-sharing probability as a function of incident energy for collisions of $Xe^{20+,30+}$ on an iron target.

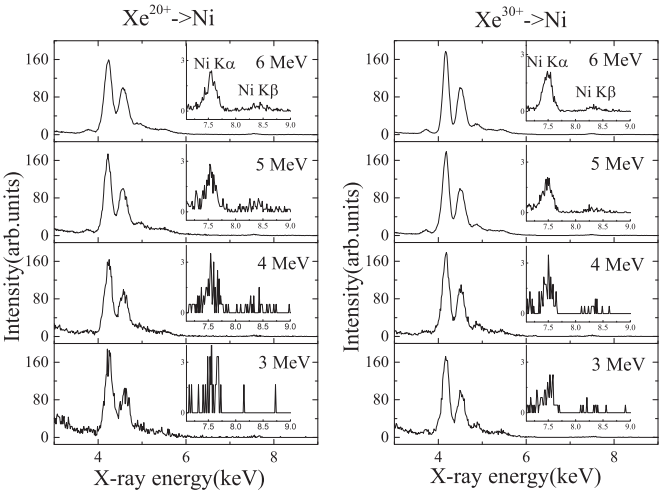

FIG. 6. Spectra for $Xe^{20+,30+}$ impacting on a nickel target with various incident energies.

Fig. 4, since the ratio and sharing probability P are positively correlated according to Eqs. (1) and (2).

In Fig. 5(b), it is shown that with the rising of incident energy, the vacancy-sharing probability P increases sharply with the incident energy for Xe^{30+}. This will lead to an increasing target-to-projectile vacancy-production cross-section ratio according to Eqs. (1) and (2). The expectation is in agreement with the experimental result that the target-to-projectile ratio increases with rising incident energy in Fig. 4. The obvious increase of the ratio for Xe^{30+} implies that the vacancy-sharing mechanism is significant for this case due to the small energy gap between the projectile L shell and target K shell. Comparatively, the vacancy-sharing probability of Xe^{20+} is much lower in magnitude since the energy gap is much larger. The vacancy-sharing process is not so important for this case. That is why the experimental results agree with the Coulomb ionization theory well in magnitude. Since changing the target atomic number is another way to adjust the energy level besides varying the charge state, we choose Xe + Ni to verify the importance of the level matching.

The spectra for the Ni target induced by Xe^{20+} and Xe^{30+} with various energies are shown in Fig. 6. No obvious charge-state effect is observed in the results because Xe + Ni is far away from the K-L level-matching region. This implies again the importance of the level matching for the inner-shell process. A suitable choice of the collision system is very important for the observance of the charge-state effect.

B. Equilibration time

Taking both the Coulomb ionization and vacancy-sharing mechanisms into account, the experimentally measured iron K x-ray yield can be written as

$$Y_{\mathrm{Fe}} = Y_{\mathrm{pre}} + Y_{eq} = Y_{\mathrm{sharing}} + Y_{DI} + Y_{eq}, \tag{5}$$

where Y_{pre} and Y_{eq} are the x-ray yields induced in the preequilibrium and equilibrium stages, respectively, and Y_{sharing} and Y_{DI} are the x-ray yields produced by vacancy-sharing and direct ionization processes, respectively, in the preequilibrium stage.

Since the equilibrium charge state is independent of the initial charge state, the observed charge-state effect for the Xe + Fe collision system originates from the collisions in the pre-equilibrium stage. Here we assume that the Coulomb ionization in the iron K-shell vacancy production process is independent of the charge state; then the difference in the iron K x-ray emissions for Xe^{30+} and Xe^{20+} bombardment is due to the first term in Eq. (5), which can be written as

$$Y_{\mathrm{sharing}} = \int_0^{\mathrm{Lpre}} P\sigma_{3d\sigma}\omega_{\mathrm{Fe}-K}N\delta L, \tag{6}$$

where L_{pre} is the preequilibrium length, P is the vacancy-sharing probability, $\omega_{(\mathrm{Fe}-K)}$ is the fluorescence coefficient for the Fe K shell, and N is the atomic density. Assuming that in the preequilibrium length, the projectile keeps its initial charge state and the energy loss is negligible, the iron x-ray yield produced by vacancy sharing Y_{sharing} can be written as

$$Y_{\mathrm{sharing}} = P\sigma_{3d\sigma}\omega_{\mathrm{Fe}-K}N\nu_p\tau, \tag{7}$$

where ν_p is the projectile velocity, τ is the equilibration time, and ν_p times τ is the preequilibrium length L_{pre}. Y_{sharing} is the mutual product of the sharing probability, vacancy-production cross section of the $3d\sigma$ MO, and the preequilibrium length.

In the present paper, the atomic fluorescence coefficient is used in the conversion of the x-ray-production cross section to the vacancy-production cross section. In a recent paper [39], the energy shift of Xe L lines was investigated, and that work presents a shift of about 60 eV to higher x-ray energy in the present collision system. Since removal of each $2p$ or $2s$ electron causes a line shift of 90 eV and removal of each $3d$ or $3p$ or $3s$ electron causes a line shift of 13 eV for LM lines, it can be estimated that the collision causes no more than one L-shell vacancy and fewer than 5 M-shell vacancies on average. Therefore it is reasonable to use the atomic value of fluorescence yield in the conversion from x-ray to vacancy production.

As for the $3d\sigma$ vacancy-production cross section, due to the very small vacancy sharing P for Xe^{20+} impacting, the Xe L-vacancy-production cross section $\sigma_{\mathrm{Xe}}^{20+}$ is approximately equal to $\sigma_{3d\sigma}$ according to Eqs. (1) and (2). Therefore, the value of $\sigma_{\mathrm{Xe}}^{20+}$ can be approximately used as the $3d\sigma$ vacancy-production cross section.

Since it can be seen from Fig. 5(b) that the sharing probability for Xe^{30+} bombardment is larger than that for Xe^{20+} by one to two orders of magnitude in the investigated energy region, it is reasonable to neglect the iron K x-ray emission from vacancy sharing for Xe^{20+}. Then the measured x-ray yield for Xe^{30+} includes an additional term Y_{sharing} in comparison with the collision of Xe^{20+} impacting. This means Y_{sharing} for Xe^{30+} impacting can be considered the difference between the experimentally measured iron K x-ray yield Y_{Fe}^{30+} for Xe^{30+} and Y_{Fe}^{20+} for Xe^{20+} bombardment.

The projectile L and target K x-ray yields for Xe^{20+} and Xe^{30+} bombardment are shown in Fig. 7. It can be seen that in the low-energy region, the Xe L x-ray emission yield for the two charge states is nearly the same, while as the incident energy is increased, the yield for Xe^{30+} becomes lower than that for Xe^{20+} and the yield gap increases slowly with the rising energy. According to Eq. (2) and Fig. 5(b), this can be

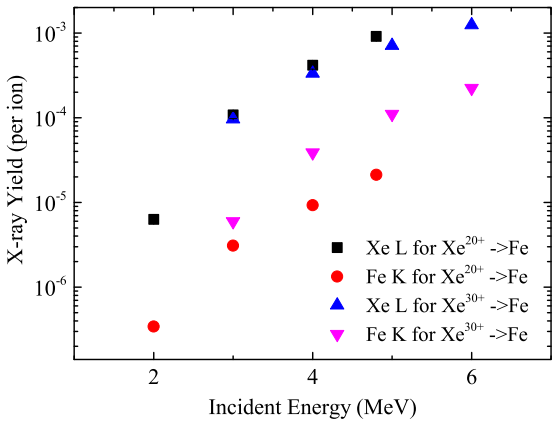

FIG. 7. (Color online) X-ray emission yield per incident ion in the collision of $Xe^{20+,30+}$ on an iron target.

explained by the increasing sharing probability gap between Xe^{20+} and Xe^{30+} bombardments.

Based on the iron K x-ray yields shown in Fig. 7 and the approximation of $\sigma_{3d\sigma} \cong \sigma_{Xe}^{20+}$ and $Y_{sharing} \cong Y_{Fe}^{30+} - Y_{Fe}^{20+}$ for the case of Xe^{30+} impacting, the preequilibrium length L_{pre} and equilibration time τ of Xe^{30+} in solid iron are calculated according to Eq. (7) and listed in Table 1. The preequilibrium length in the present energy region is about hundreds of atomic layers, and the equilibration time is about 9 fs. The obtained equilibration time agrees in magnitude with the results of Hattass *et al.* [26], which is around 7 fs.

IV. CONCLUSION

In summary, we have measured the charge-state and incident energy dependence of the x-ray emission in the interaction of xenon ions with thick solid targets. In heavy-ion-atom collision systems near the level-matching region such as Xe + Fe, the x-ray emission greatly depends on the projectile charge state, and the vacancy-sharing theory gives a good description of the vacancy-production process.

The observed apparent charge-state effect for Xe + Fe originates from the collision in the preequilibrium stage. From the data, the equilibration time τ is derived to be around 9 fs, and the preequilibrium length is about hundreds of atomic layers. We conclude that the large sharing probability of 0.144, large $3d\sigma$ vacancy-production cross section, and the collision of hundreds of atomic layers in the preequilibrium stage act mutually to make $Y_{sharing}$ significant enough to be observed in the experiment for Xe^{30+} bombardment.

TABLE I. Preequilibrium length and equilibration time deduced from Eq. (7) for Xe^{30+} ions on Fe. The typical uncertainty is 15%, which originates from the stopping-power uncertainty, incident ion statistic, and the fitting error.

E (MeV)	L_{pre} (nm)	τ (fs)
4	22.2 ± 3.3	9.1 ± 1.4
4.8	23.4 ± 3.5	8.7 ± 1.3
5	23.1 ± 3.5	8.5 ± 1.3
6	27.8 ± 4.2	9.3 ± 1.4

The investigation in the present paper is in the charge-state region before the exact level-matching peak; further studies involving either higher charge states or a lower target atomic number to make the collision system approach or exceed the level-matching peak are highly desirable.

The evolution of the charge state of highly charged ions in solid is still unclear. In the future, with a depth-scanning technique, the depth dependence of the x-ray emission can be obtained. Since, in the level-matching region, the x-ray emission is highly sensitive to the charge state, the charge-state evolution can be obtained through the x-ray emission measurement.

ACKNOWLEDGMENTS

We truly appreciate the help of the staffs of the 320 kV ECR platform in IMP-Lanzhou for providing ion beams during the experiment. The work is supported by the National Basic Research Program of China (Grant No. 2010CB832902) and the National Natural Science Foundation of China (Grants No. 11205225, No. 11505248, No. 11105192, No. 11275238, No. U1532263, and No. 11275241).

[1] M. Barat and W. Lichten, Phys. Rev. A **6**, 211 (1972).
[2] J. Eichler, U. Wille, B. Fastrup, and K. Taulbjerg, Phys. Rev. A **14**, 707 (1976).
[3] J. H. McGuire and P. Richard, Phys. Rev. A **8**, 1374 (1973).
[4] J. D. Garcia, R. J. Fortner, and T. M. Kavanagh, Rev. Mod. Phys. **45**, 111 (1973).
[5] V. Horvat, R. L. Watson, and Y. Peng, Phys. Rev. A **79**, 012708 (2009).
[6] R. L. Watson, V. Horvat, and Y. Peng, Phys. Rev. A **78**, 062702 (2008).
[7] R. L. Watson, Y. Peng, V. Horvat, and A. N. Perumal, Phys. Rev. A **74**, 062709 (2006).
[8] R. L. Watson, J. M. Blackadar, and V. Horvat, Phys. Rev. A **60**, 2959 (1999).
[9] R. Anholt, W. E. Meyerhof, Ch. Stoller, E. Morenzoni, S. A. Andriamonje, J. D. Molitoris, O. K. Baker, D. H. H. Hoffmann, H. Bowman, J.-S. Xu, Z.-Z. Xu, K. Frankel, D. Murphy, K. Crowe, and J. O. Rasmussen, Phys. Rev. A **30**, 2234 (1984).
[10] P. M. Mokler, D. H. H. Hoffmann, W. A. Schönfeldt, D. Maor, W. E. Meyerhof, and Z. Stachura, Nucl. Instrum. Methods Phys. Res., Sect. B **4**, 34 (1984).
[11] A. Schmiedekamp, T. J. Gray, B. L. Doyle, and U. Schiebel, Phys. Rev. A **19**, 2167 (1979).
[12] H. O. Lutz, J. Stein, S. Datz, and C. D. Moak, Phys. Rev. Lett. **28**, 8 (1972).
[13] T. Schlathölter, A. Närmann, A. Robin, D. F. A. Winters, S. Marini, R. Morgenstern, and R. Hoekstra, Phys. Rev. A **62**, 042901 (2000).

[14] N. Stolterfoht, A. Arnau, M. Grether, R. Köhrbrück, A. Spieler, R. Page, A. Saal, J. Thomaschewski, and J. Bleck-Neuhaus, Phys. Rev. A **52**, 445 (1995).
[15] S. Schippers, S. Hustedt, W. Heiland, R. Köhrbrück, J. Bleck-Neuhaus, J. Kemmler, D. Lecler, and N. Stolterfoht, Phys. Rev. A **46**, 4003 (1992).
[16] W. E. Meyerhof, A. Rüetschi, C. Stoller, M. Stockli, and W. Wölfli, Phys. Rev. A **20**, 154 (1979).
[17] W. E. Meyerhof, R. Anholt, and T. K. Saylor, Phys. Rev. A **16**, 169 (1977).
[18] R. Anholt and W. E. Meyerhof, Phys. Rev. A **16**, 190 (1977).
[19] W. E. Meyerhof, R. Anholt, T. K. Saylor, S. M. Lazarus, A. Little, and L. F. Chase, Phys. Rev. A **14**, 1653 (1976).
[20] J. Ren, Y. Zhao, X. Zhou, R. Cheng, Y. Lei, Y. Sun, X. Wang, G. Xu, Y. Wang, S. Liu, Y. Yu, Y. Li, X. Zhang, Z. Xu, and G. Xiao, Phys. Scr. **T156**, 014036 (2013).
[21] P. H. Mokler, D. H. H. Hoffmann, W. A. Schonfeldt, D. Maor, and Z. Stachura, J. Phys. B **17**, 4499 (1984).
[22] A. Warczak, D. Liesen, P. H. Mokler, and W. A. Schonfeldt, J. Phys. B **14**, 1315 (1981).
[23] W. N. Lennard, I. V. Mitchell, G. C. Ball, and P. H. Mokler, Phys. Rev. A **23**, 2260 (1981).
[24] A. Warczak, D. Liesen, J. R. Macdonald, and P. H. Mokler, Z. Phys. A **285**, 235 (1978).
[25] W. A. Schönfeldt, P. H. Mokler, D. H. H. Hoffmann, and A. Warczek, Z. Phys. D **4**, 161 (1986).
[26] M. Hattass, T. Schenkel, A. V. Hamza, A. V. Barnes, M. W. Newman, J. W. McDonald, T. R. Niedermayr, G. A. Machicoane, and D. H. Schneider, Phys. Rev. Lett. **82**, 4795 (1999).
[27] R. Herrmann, C. L. Cocke, J. Ullrich, S. Hagmann, M. Stoeckli, and H. Schmidt-Boecking, Phys. Rev. A **50**, 1435 (1994).
[28] Y. Fang, G. Xiao, H. Xu, Z. Sun, Y. Zhao, Z. Hu, H. Xu, T. Huang, and Y. Wang, Chin. Phys. B **17**, 148 (2008).
[29] X. Zhou, Y. Zhao, R. Cheng, Y. Wang, Y. Lei, X. Wang, and Y. Sun, Nucl. Instrum. Methods Phys. Res., Sect. B **299**, 61 (2013).
[30] K. Taulbjerg and P. Sigmund, Phys. Rev. A **5**, 1285 (1972).
[31] M. Gryziński, Phys. Rev. **138**, A336 (1965).
[32] C. Foster, T. P. Hoogkamer, P. Woerlee, and F. W. Saris, J. Phys. B **9**, 1943 (1976).
[33] J. S. Hansen, Phys. Rev. A **8**, 822 (1973).
[34] W. E. Meyerhof, Phys. Rev. A **18**, 414 (1978).
[35] P. Kurpick, T. Bastug, W.-D. Sepp, and B. Fricke, Phys. Rev. A **52**, 2132 (1995).
[36] L. Sarkadiy, T. Mukoyamaz, and Z. Smit, J. Phys. B **29**, 2253 (1996).
[37] W. E. Meyerhof, R. Anholt, J. Eichler, and A. Salop, Phys. Rev. A **17**, 108 (1978).
[38] E. E. Nikitin, Adv. Quantum Chem. **5**, 135 (1970).
[39] X. Zhou, Y. Zhao, R. Cheng, X. Wang, J. Ren, Y. Lei, Y. Sun, G. Xu, Y. Wang, and G. Xiao, Nucl. Instrum. Methods Phys. Res., Sect. B **304**, 32 (2013).